ACS APPLIED ELECTRONIC MATERIALS

pubs.acs.org/acsaelm
Article

Chemical, Structural, and Electrical Changes in Molecular Layer-Deposited Hafnicone Thin Films after Thermal Processing

Vamseedhara Vemuri, Sean W. King, Ryan Thorpe, Andrew H. Jones, John T. Gaskins, Patrick E. Hopkins, and Nicholas C. Strandwitz*

Cite This: ACS Appl. Electron. Mater. 2024, 6, 5173−5182
Read Online

ABSTRACT: Post deposition annealing of molecular layer-deposited (MLD) hafnicone films was examined and compared to that of hafnium oxide atomic layer-deposited (ALD) films. Hafnicone films were deposited using tetrakis(dimethylamido)-hafnium (TDMAH), and ethylene glycol and hafnia films were deposited using TDMAH and water at 120 °C. The changes in the properties of the as-deposited hafnicone films with annealing were probed by various techniques and then compared to the as-deposited and annealed ALD hafnia films. In situ X-ray reflectivity indicated a 70% decrease in thickness and ∼100% increase in density upon heating to 400 °C yet the density remained lower than that of hafnia control samples. The largest decreases in thickness of the hafnicone films were observed from 150 to 350 °C. In situ X-ray diffraction indicated an increase in the temperature required for crystallization in the hafnicone films (600 °C) relative to the hafnia films (350 °C). The changes in chemistry of the hafnicone films annealed with and without UV exposure were probed using Fourier transformed infrared spectroscopy and X-ray photoelectron spectroscopy with no significant differences attributed to the UV exposure. The hafnicone films exhibited lower dielectric constants than hafnia control samples over the entire temperature range examined. The CF_4/O_2 etch rate of the hafnicone films was comparable to the etch rate of hafnia films after annealing at 350 °C. The thermal conductivity of the hafnicone films initially decreased with thermal processing (up to 250 °C) and then increased (350 °C), likely due to porosity generation and subsequent densification, respectively. This work demonstrates that annealing MLD films is a promising strategy for generating thin films with a low density and relative permittivity.

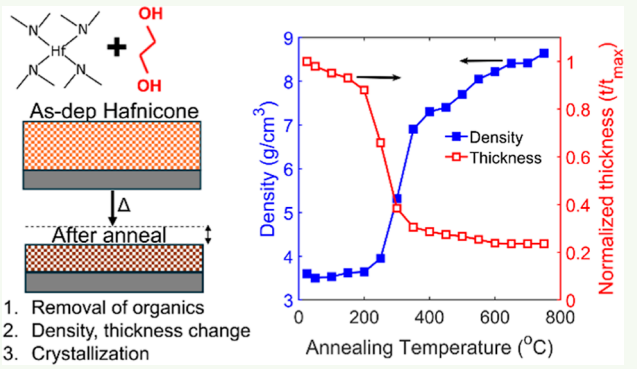

KEYWORDS: *ALD, MLD, hybrid films, thermal processing, low-k, etch stops, annealing, thin films*

INTRODUCTION

With the ultimate goal of continuously increasing the efficiency and processing speed of electronics, much emphasis has been placed on fabricating smaller transistors with new geometries.[1,2] Miniaturization of transistors has led to a decrease in the overall size of components and connections within integrated circuits (ICs), thus enabling a rapid increase in density of the components in an IC. This miniaturization of the components in the IC (scaling) introduces resistance and capacitance (RC) delays, which are parasitic to performance.[3,4] The resistance and capacitance delays arise from the metal interconnects and the interlayer dielectrics (ILD)/etch stops, respectively. To decrease the resistance, the resistivity of the conducting material can be decreased, whereas the capacitance delays can be decreased by decreasing the dielectric constant of the ILD and etch stops.[4,5]

Currently, SiOCH is used as an ILD, whereas SiC (k = 4−7),[6−10] SiN (k = 6.5−7),[11−13] and SiCN (k = 4.5−5.8)[14−17] are common etch stop materials that are deposited using plasma-enhanced chemical vapor deposition (PECVD).[18] Matrix forming precursors like diethoxymethylsilane and triethoxymethylsilane and porogens like α-terpinene and cinene are employed to deposit low-k films whose density can be modified by subjecting the films to post deposition annealing.[19] Post deposition anneal parameters including anneal time, UV wavelength, and temperature affect density and porosity.[20,21] In addition to having low k values, the etch stops should also act as a diffusion barrier to prevent the diffusion of copper into the ILD.[18] Since diffusion of Cu is faster through grain boundaries, amorphous films are preferred for ILD and etch stop layers.[22] The plasma can sometimes damage the dielectric films during PECVD, motivating the use of nonplasma processes.[23−25] Hence, deposition methods that

Received: April 17, 2024
Revised: June 13, 2024
Accepted: June 13, 2024
Published: June 28, 2024

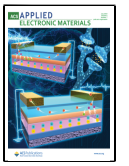

minimize the ion-induced damage and can provide new materials that can replace the conventional Si-based dielectrics to decrease the RC delays while providing etch contrast to Si-based materials (i.e., etch stops) are of interest.

Atomic layer deposition (ALD) can deposit conformal thin films on high aspect ratio structures at low temperatures in a layer-by-layer fashion and is already used in IC manufacturing.[26] For example, ALD hafnia is used as a high-k gate dielectric in transistors.[27] Hafnia also has different wet and dry etch behavior compared to Si-based dielectrics, motivating its potential use in etch stop layers within the ILD. However, hafnia deposited by ALD has a low crystallization temperature (350−400 °C) and high dielectric constant (k > 10), thus making it potentially unsuitable for low-k layers.[28−30] If the dielectric constant of the ALD hafnia could be decreased while maintaining other attributes, such as low etch rates and retaining an amorphous structure at typical processing temperatures (∼400 °C), it may constitute an alternate low-k component layer in etch stop applications.

Molecular layer deposition (MLD) is an analogue of ALD where molecular fragments are included in the resulting films and may be a route to porous and/or low-k materials.[31,32] In prior studies, chemical changes in MLD metalcone films were observed with UV, thermal, and/or ambient exposure, indicating the removal of organics and changes in physical properties.[33−38] Previously, aluminum oxide-based materials were developed for low-k etch stop applications motivating us to explore the applicability of hafnium-based MLD films for the low-k applications and to better understand the synthesis−structure−composition−property relationships in these materials.[32,39,40] In this work, we deposit hafnicone, which is a hybrid hafnium alkoxide film,[41] using MLD and report the thermally induced removal of the organic components and the ability to create low density and low k films relative to HfO_2. We examine the evolution of chemical, structural, and electrical properties of the as-deposited and annealed hafnicone films in comparison to those of ALD hafnia films.

EXPERIMENTAL METHODS

Hafnicone films were deposited using a viscous flow reactor that is described in-detail elsewhere.[42] Research grade N_2 (99.9999%, Airgas) was used as the carrier gas, and the flow rate was 60 sccm under continuous pumping that resulted in a base pressure of 250 mTorr during the growth. The walls of the reactor were heated to 120 °C, and the precursor manifold, precursor delivery line, and the stop valve between the vacuum pump and sample chamber were heated to 150 °C. Hafnicone precursors included tetrakis(dimethylamido) hafnium (TDMAH, 99%, STREM chemicals) and ethylene glycol (EG, 99%, Sigma-Aldrich). Hafnia control samples were deposited using TDMAH and 18.2 MΩ water. The films were deposited on test-grade (100) p-Si wafers with a thin native oxide. Si wafers were first cleaned by sonicating sequentially in isopropanol and water. The hafnicone films were grown using two 0.2 s TDMAH pulses using a vapor draw configuration separated by 10 s purge (N_2) followed by 0.6 s EG pulse using a boost system and 60 s purge time between TDMAH and EG doses. The precursor boost system pressurizes the vapor-drawn precursor cylinder with N_2 at ∼20 psig prior to pulsing the vapor contents (N_2 and EG in this case) into the chamber. A quartz crystal microbalance (QCM) was used to monitor the growth rate of the films. A detailed summary of the QCM is described elsewhere.[42] The crystal surface was first conditioned with 25 cycles of ALD alumina (trimethylaluminum and water) before starting the growth to have a uniform oxide surface.

A custom-built UV chamber (172 nm) was used to anneal the as-deposited (120 °C) hafnicone films at 150, 250, or 350 °C for 10 min either with or without UV irradiation in the N_2 atmosphere.[32] In this case, UV light was blocked from some of the samples during heating, whereas some samples were exposed to UV light. The pressure of the UV chamber was controlled by a needle valve and held at 90 mTorr.

The film thicknesses were measured by fitting spectroscopic ellipsometry (SE) data collected with a Woollam VASE spectroscopic ellipsometer. A Cauchy model was used to fit the data and determine the thickness and other optical constants in CompleteEASE software. The Maxwell-Garnett method in effective medium approximation (EMA) was used to calculate the void percentage also in CompleteEase. Capacitance−voltage (C−V) measurements were conducted by fabricating metal-oxide-semiconductor capacitors (MOSCAPs). For MOSCAPs, films were grown on prime grade (100) p-Si (1−10 Ω-cm). The p-Si wafers were cleaved to 1.5 × 1.5 cm^2 pieces and were cleaned by sonicating sequentially in isopropanol and water. Samples were then subjected to Radio Corporation of America (RCA) cleaning 1 and 2.[43] After RCA cleaning, the samples were hydrogen-terminated to remove the native silicon oxide layer by immersion in 5 wt % hydrofluoric acid (Transene, Inc.) for 1 min followed by rinsing with water and drying under a filtered $N_2(g)$ stream. A HP4194A impedance analyzer and mercury probe (MDC 802B) were used to perform the C−V measurements. The dielectric constant of the MOSCAP test structures was extracted using $C = \frac{k\varepsilon_0 A}{t}$, where C is the capacitance of the film, k is the dielectric constant, ε_0 is the permittivity of free space, A is the area of the mercury drop, and t is the thickness of the film.

FTIR spectra of the hafnicone films were obtained by depositing the films on 2 × 6.5 cm^2 double side polished (DSP) float zone Si(100) from Virginia Semiconductor or DSP test grade Si wafer from University Wafer. The DSP Si wafers were cleaned by sonicating sequentially in isopropanol and 18.2 MΩ water followed by 5 min of UV−ozone (UVO) treatment (Jelight). The FTIR measurements were performed in the transmission mode using a PerkinElmer Spectrum 100 spectrometer under a N_2 purge. The FTIR background spectrum was collected from the substrate after cleaning but prior to film growth to isolate the signal from the film. The spectra were collected from 750 to 4000 cm^{-1} and averaged over 250 scans by using a resolution of 4 cm^{-1}.

X-ray reflectivity (XRR) and X-ray diffraction (XRD) measurements used a PANalytical Empyrean X-ray diffractometer with a Cu X-ray tube with a wavelength of 1.54 Å. The in situ XRR and XRD measurements used a DHS 1100 (Anton Paar) heating stage in air ambient from 50 to 750 °C at 50 °C intervals. The XRR data were fit to quantify the film density and thickness using X'pert reflectivity software. In situ XRR and XRD data were obtained from hafnicone films deposited on 1.5 × 1.5 cm^2 thermal oxide (500 nm) Si substrates to minimize difficulties in thickness estimation due to the growth of interfacial silicon oxide that would occur in native-oxide Si substrates during heating, whereas the ex situ experiments are carried out on 1.5 × 1.5 cm^2 test-grade (100) p-Si with a thin native oxide (∼1.5 nm).

X-ray photoelectron spectroscopy (XPS) was conducted using SPECS XPS instrument using a photon energy of 1486.6 eV. The pass energy for all core level scans was 20 eV, and the pass energy for the survey scans was 70 eV. Binding energy correction of all data was carried out by normalization to the C 1s peak at 284.8 eV. This type of binding energy correction is known to have an error of a few tenths of an eV when used for insulating samples like hafnia and represents a source of uncertainty in all XPS measurements in this work.[44] The O 1s peak was deemed unsuitable as a binding energy reference due to the presence of several O chemical states at similar binding energies.

Films were etched using a Technics MICRO-RIE series 800 system in a mixture of 96% CF_4 and 4% w/v O_2. The conditions included 250 W power, and the gas flow was set to maintain a base pressure of 200 mTorr. The samples were etched for 2 min, and the etch rate was calculated by measuring the thickness before and after etching using SE.

Steady-state thermoreflectance was used to quantify the thermal conductivity of the hafnicone films. The samples were coated with an optically opaque aluminum film, and then a pump laser light source

https://doi.org/10.1021/acsaelm.4c00683
ACS Appl. Electron. Mater. 2024, 6, 5173−5182

was used to heat the sample surface while another laser light was used as a probe to measure the changes in the reflectivity related to the pump-induced steady-state temperature rise. The relationship between the pump power and the resulting changes in reflectivity were used to calculate the thermal conductivity of the films.[45−47] The effective thermal conductivity of the hafnicone films was calculated by first determining the thermal conductivity of the substrate and the thermal boundary resistance (TBR) of the UVO-grown silicon oxide. The TBR of the UVO-grown silicon oxide was subtracted from the total measured TBR of the hafnicone film stacks, and the film thickness was divided by the difference to determine the effective thermal conductivity of the hafnicone films. This technique has been explained in detail elsewhere.[48]

RESULTS AND DISCUSSION

The growth behavior including the growth rate per cycle and data from in situ QCM measurements were generally consistent with prior studies of hafnicone [Hf(EG)] growth.[41,49] The in situ QCM data displayed a linear increase in mass with an increasing number of cycles (Figure S1) for Hf(EG) films grown at 120 °C. The average mass gain over 100 cycles was 37 ng/cm^2/cycle, and the growth per cycle (GPC) of hafnicone films grown at 120 °C was 1.23 Å/cycle, as determined by SE. The GPC of hafnicone films has previously been shown to vary from 0.7 to 1.5 Å/cycle depending on the growth temperature from 100 to 150 °C, where higher temperatures showed lower growth rates.[35,41,50] The average mass gain/cycle observed for hafnicone films by QCM in prior studies grown at 145 °C was 17 ng/cm^2/cycle.[41] The reason for the higher average mass gain/cycle may be the lower growth temperature (120 °C) used in our case. The density calculated using QCM was 3.25 g/cm^3 and was obtained by using the thickness from SE and the mass gain per area from QCM. This value is similar to the density fit from XRR of the as-grown films in the present work (3.4 g/cm^3). The density obtained in our case using QCM is slightly higher than the reported literature value of 3 g/cm^3 observed using XRR from 100 to 205 °C.[41]

The hafnia and hafnicone films were annealed up to 750 °C, and their density and thickness were estimated from in situ XRR measurements (Figure 1). The hafnia films showed a 10% thickness decrease after crystallization at 400 °C, as determined through separate XRD experiments (marked by the single arrow, Figure 1a) and then remained constant, whereas the hafnicone films undergo a 78% thickness decrease after annealing to 750 °C. The largest decrease in thickness of the hafnicone films was observed between 200 and 350 °C.

The density of 3.5 g/cm^3 in the as-deposited films quantified by in situ XRR measurement was similar to the film density value obtained using QCM (3.25 g/cm^3). The density of the as-deposited and annealed hafnicone films deposited at 120 °C was lower than the as-deposited and annealed hafnia films from 50 to 750 °C. The density of hafnia films gradually increased from 9 to 9.5 g/cm^3 after 750 °C anneal (∼5% increase), whereas the density of hafnicone films increased from 3.42 to 8.2 g/cm^3 over this same temperature range (∼135% increase). At 750 °C, the density of hafnicone films (8.2 g/cm^3) was 16% lower than the density of the hafnia (9.5 g/cm^3) films possibly due to the presence of porosity or carbonaceous species. The rapid increase in density from 3.7 to 7 g/cm^3 and the decrease in thickness for hafnicone films were observed during 250−350 °C annealing, indicating removal of some organics and densification. This decrease in thickness and the increase in density in this temperature range could be a result of mass loss

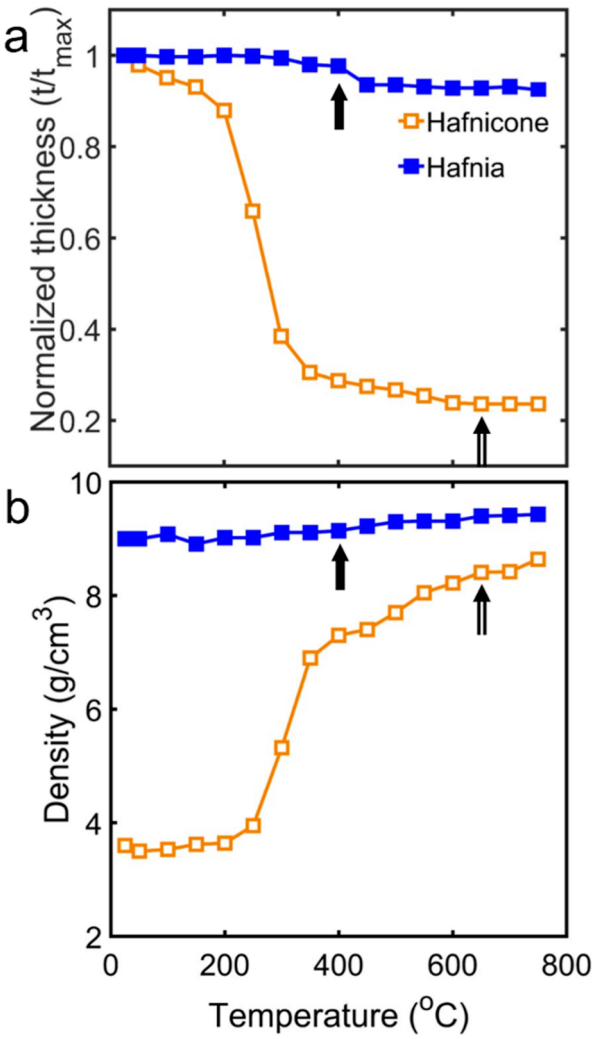

Figure 1. (a) Normalized thickness and (b) mass density as a function of annealing temperature for hafnia and Hf(EG) films derived from in situ XRR data. The solid and double arrows represent the crystallization temperatures of the hafnia and hafnicone films, respectively.

due to the removal of organics like CO, CO_2, and CH_4 in the form of volatile products, which are released due to the cleavage of C−C and C−H bonds from the EG species (HO−CH_2−CH_2−O−Hf) inside the film causing film collapse and densification.[32,51,52]

The density evolution of the hafnicone films annealed from 150 to 350 °C at 100 °C intervals both with and without UV in ambient nitrogen was measured using ex situ XRR (Figure S9). The density increased from 3.3 to 5.9 g/cm^3 after annealing from 150 to 350 °C. The UV cured samples had slightly higher density after 250 and 350 °C anneals than the samples annealed without UV. The differences in the density obtained from the in situ and ex situ measurements could be attributed to differences in heating rates and heating ambient conditions between the experiments. The porosity (void percent), refractive index (n at 500 nm), and change in thickness of the as-deposited and annealed films were calculated using the EMA (Table S6). The thickness decreased (∼50%) with annealing, and refractive index increased (18%) with annealing, whereas the changes in EMA-estimated porosity in the samples

https://doi.org/10.1021/acsaelm.4c00683
ACS Appl. Electron. Mater. 2024, 6, 5173−5182

after annealing were small for all samples and remained in the range of 18.8−20.2%.

In situ XRD was used to monitor the crystallization behavior of hafnia and hafnicone films after annealing in air from room temperature to 600 and 700 °C, respectively, at 50 °C intervals (Figure 2). The portion of the data missing was removed due

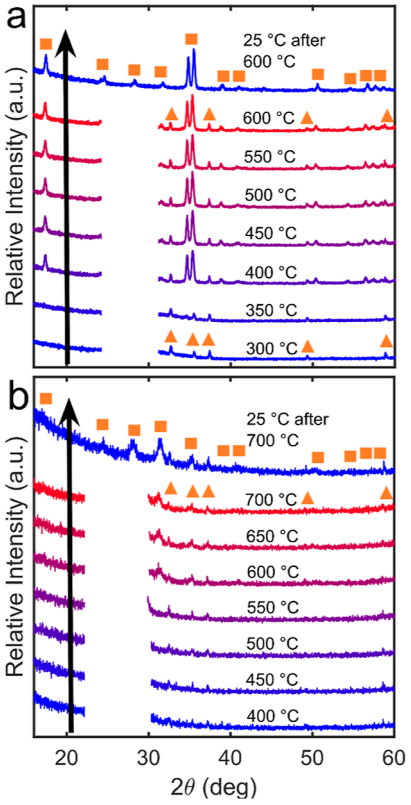

Figure 2. In situ XRD data for the (a) hafnia and (b) hafnicone films with increasing annealing temperature. Data plotted at the top of each pane was measured without the nonambient stage or dome at room temperature after heating to the maximum temperature. The arrows indicate the order in which the diffraction data were acquired. The squares indicate Bragg peak locations for monoclinic HfO_2, and the triangles indicate reflections from the sample stage. A portion of each data set was removed due to an intense reflection from the graphite heating stage dome, which was removed for the final measurement after (top plot in each pane).

to the high intensity of diffraction from the graphite dome used to enclose the sample during heating. Peaks marked with a square are attributed to monoclinic HfO_2, and those marked with a triangle are due to the nonambient stage. The hafnia films were amorphous until 400 °C, at which point the films displayed intense peaks indicating the onset of crystallization and are consistent with the monoclinic phase of hafnia.[53,54] We compared our data with those of other phases of hafnia and found that our samples were consistent with only the monoclinic polymorph. The hafnicone films did not crystallize until above 550 °C. After annealing the hafnicone films to 600 °C, a broad peak was observed at 31.4°, indicating the onset of crystallization. After the films were annealed up to 700 °C, the graphite dome was removed to observe the diffraction of hafnicone films more clearly. The observed peaks are broad and indicate the presence of nanocrystalline domains. The observed peaks are also consistent with the monoclinic phase of hafnia. The delay in the onset of crystallization in hafnicone films indicates that the presence of organics inside the film delays the crystallization by ∼200 °C. The starting thickness of the hafnia, hafnicone films before the in situ heating experiment was 58 and 54 nm, respectively, and after the in situ measurements, hafnia films showed approximately 10% decrease (53 nm) and hafnicone films showed 70% decrease (17 nm) in thickness, consistent with the in situ XRR thickness observations. The small thickness of the hafnicone films and the broadness of the peaks after thermal processing are responsible for the weak diffraction observed in these samples relative to the hafnia control samples.

The chemistry and thermal evolution of the as-deposited and annealed hafnia and hafnicone samples were probed using FTIR spectroscopy from 4000 to 500 cm^{-1} (Figure 3). In the

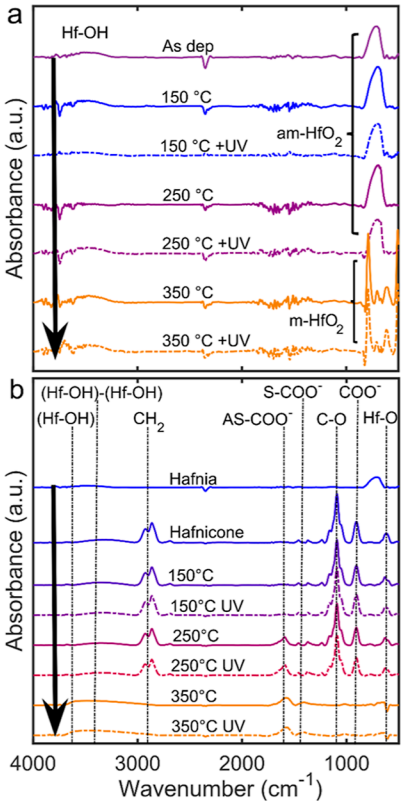

Figure 3. FTIR spectra of (a) as-deposited, thermally processed, and UV-cured hafnia films and (b) as-deposited, thermally processed, and UV-cured hafnicone films deposited at 120 °C. The peak assignments include 3650 cm^{-1}: OH; 3330 cm^{-1}: Hf−OH; 2860 and 2920 cm^{-1}: CH_x; 2350 cm^{-1}: CO_2; 1090 cm^{-1}: C−O/C−C; and 1370−900 cm^{-1}: symmetric-COO^- and COO^-.

hafnia FTIR spectra (Figure 3a), the hydroxyl peak and amorphous features of the Hf−O network are observed at 3600 and 705 cm^{-1}, respectively. Hydroxyls are incorporated and retained in the film and are observed, even after 350 °C anneal. The amorphous signature feature (500−800 cm^{-1}) transforms after 350 °C anneal to sharp intense peaks, which are the IR-active modes of crystalline monoclinic phase of hafnia.[55,56] The negative features observed around 2350 cm^{-1} correspond to the presence of atmospheric CO_2 in the instrument, indicating that CO_2 was not completely purged prior to the measurement or baseline acquisition.[57−59] No major difference in FTIR data between the samples that were annealed with and without UV light was observed. The 50 °C

https://doi.org/10.1021/acsaelm.4c00683
ACS Appl. Electron. Mater. 2024, 6, 5173−5182

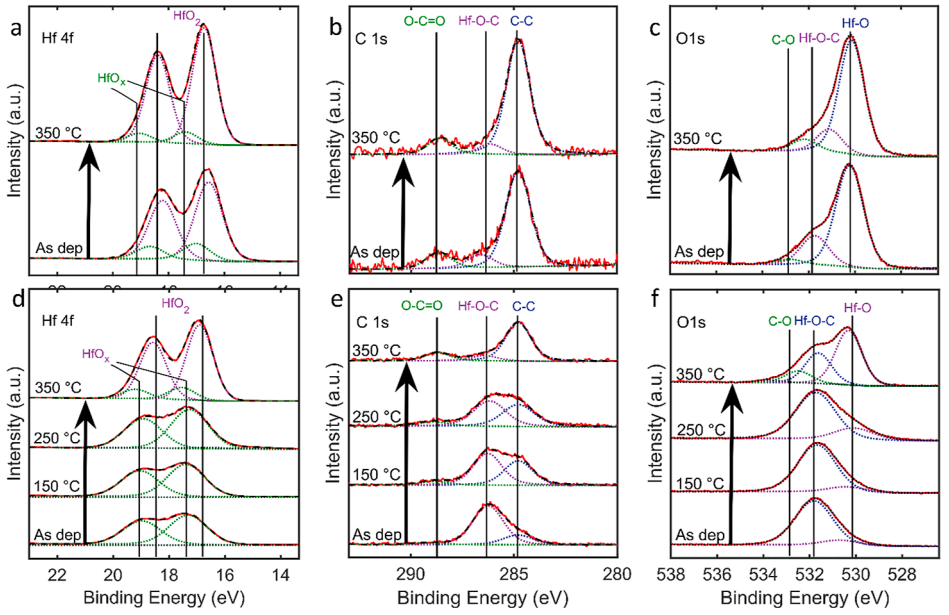

Figure 4. XPS data of the (a) Hf 4f, (b) C 1s, and (c) O 1s regions of the hafnia films deposited at 120 °C and annealed from 150 and 350 °C under vacuum and (d) Hf 4f, (e) C 1s, and (f) O 1s regions of the hafnicone films deposited at 120 °C and annealed at 150−350 °C at 100 °C intervals under vacuum. Vertical lines indicate the approximate locations of the labeled species.

difference in the crystallization temperatures of the hafnia films observed by using XRD and FTIR could be attributed to differences in the heating system, heating rates, and heating times that may affect the kinetics of hafnia crystallization.

Turning to the hafnicone films (Figure 3b), the as-deposited hafnicone films displayed absorption peaks consistent with the inclusion of EG. Peaks observed at 2860, 2920 cm^{-1} correspond to $-CH_2$ and at 1090 cm^{-1} correspond to C−O/C−C species.[32] These peaks are consistent with the presence of metal−alkoxide bonds. The broad feature at 3330 cm^{-1} corresponds to the hydrogen bond between Hf−OH and Hf−OH species.[55] The peaks at 1370 and 900 cm^{-1} correspond to the presence of COO^- carboxylate species.[33] The presence of hydroxyl and carboxylate peaks in the as-deposited sample may correspond to the slight oxidation of the samples due to the uptake of moisture from the atmosphere. Upon annealing up to 250 °C, the intensity of $-CH_2$ peaks at 2860 and 2920 cm^{-1} and intensity of C−O peaks at 1090 cm^{-1} decrease. After annealing hafnicone at 250 °C, new peaks around 1400−1700 cm^{-1} appear corresponding to the formation of free water or, more likely, asymmetric COO^- species and the intensity of CH_2 and C−O features decrease. After the 350 °C anneal, the weak feature around 1400−1700 cm^{-1} becomes more intense (more clearly visible in Figure S2), and the CH_2 peak disappears possibly indicating the formation of carboxylate species due to the cleavage and oxidation of the alkoxides (CH_2, C−O) from the EG linker and desorption of EG (these changes are also emphasized in FTIR difference spectra in Figure S3).[33−35] Only minor differences between the films that were annealed and those annealed under UV irradiation were observed. No evidence of crystalline HfO_2 was observed in the FTIR spectra upon heating up to 350 °C, consistent with the XRD observations that the films remain amorphous up to ∼600 °C.

To quantify the changes in the concentration of species contributing to the IR spectra (CH_2, C−O, and OH) after thermal processing, the area under the curve for these absorption features was normalized to the film thickness after each annealing step (Figure S4). Nearly all of the C−O species and up to 80% of the CH_x species were removed from the film after heating to 350 °C. The concentration of the O−H species decreased ∼20% after 150 °C annealing and then increased to 160% of the initial value after 350 °C annealing, indicating that new hydroxyl species are generated inside the film. After 250 °C anneal, COO^- species are generated inside the film, and the intensity of CH_x and C−C/C−O decreases further. After 350 °C anneal, most of the CH_x and C−C/C−O peaks disappear, whereas new −OH species appear and the COO− features become more intense.

The chemical transformations of the hafnicone and hafnia films were characterized by using XPS (Figure 4). Figure 4a shows the Hf 4f core level of hafnia films in the as-deposited state and after annealing at 350 °C with the expected splitting due to spin−orbit coupling. The energy separation of these 4f peaks is 1.67 eV for all chemical states, and the ratio of their areas is 4:3.[60] For the sake of simplicity, only the $4f_{7/2}$ components are discussed here. The most intense peak in this spectrum is at 16.7 eV, which is consistent with stoichiometric HfO_2.[61,62] The best fit to this spectrum was achieved by adding a second component at 17.4 eV. This additional chemical state could be due to surface states, defects, or carbon bound to the surface of the film. After annealing to 350 °C, the HfO_2 peaks became more intense. The peak positions also shifted to a slightly higher binding energy, but this is within the margin of error of the experiment, as discussed in the Section Experimental Methods.

The corresponding C 1s spectra from this sample are shown in Figure 4b. Before and after annealing, these spectra exhibit three components at 284.8, 286.2, and 288.6 eV, which can be attributed to C−C, C−O, and O−C═O bonding, respectively. These chemical states are characteristic of adventitious carbon contamination, which is commonly found in the XPS spectra of samples that have not been cleaned in situ before performing measurements. The FTIR spectra of hafnia films in Figure 3a do not display the CH_x peaks at 3000 cm^{-1},

https://doi.org/10.1021/acsaelm.4c00683
ACS Appl. Electron. Mater. 2024, 6, 5173−5182

indicating that the C observed in XPS of hafnia films is likely adventitious and surface bound.

The O 1s spectra of the as-deposited and annealed hafnia films are shown in Figure 4c. These spectra display an intense peak around 530 eV corresponding to Hf−O and a smaller, broader peak around 532 eV from O−H or Hf−O−C bonding (Figure 4f).[63,64] The intensity of the peak at 532 eV (O−H, Hf−O−C) decreases after annealing possibly indicating condensation of neighboring OH species forming HfO_2.

Figure 4d−f shows the Hf 4f, C 1s, and O 1s spectra from the hafnicone films. The main Hf 4f component in the as-deposited spectrum is present at 17.3 eV and can be attributed to Hf−O−C bonding. This peak assignment is supported by the large C−O peaks in both the C 1s (286.2 eV) and O 1s (532 eV) spectra. The presence of O−C═O species in the as-deposited hafnicone sample may correspond to the slight oxidation of the hafnicone films before the analysis as supported by the hydroxyl peak (3330 cm^{-1}) from the FTIR (Figure 3b), which is commonly observed in metalcone films after exposure to air.[65] The spectra show minimal changes at 150 and 250 °C. However, after annealing at 350 °C, the Hf−O−C peaks in the Hf 4f spectrum decrease substantially, while new components appear at 16.7 eV, suggesting that the hafnicone has transformed into HfO_2. This suggestion is further supported by the similarity of the 350 °C hafnicone sample to the hafnia samples (Figure 4a).

The C 1s and O 1s spectra similarly show a decrease in C−O bonding and an increase in Hf−O. The O 1s spectra of the as-deposited hafnicone films had a peak at 532 eV corresponding to Hf−O−C and adventitious O−H and a peak at 530.8 eV corresponding to the Hf−O bonding (Figure 4f).[64,66] With increasing annealing temperature and cleavage of Hf−O−C bonds, the films may form a substoichiometric oxide comprising Hf^{3+} up to 250 °C, which is then converted to HfO_2 with 1.8:1 stoichiometry after the 350 °C anneal.[67,68] After annealing at 350 °C, the intensity of the Hf−O−C feature (from Hf 4f and C 1s) decreases while the intensity of C−C and O−C═O features (from C 1s) increases likely due to the cleavage of the Hf−O−CH_2−CH_2−O−Hf species and some carbonaceous species polymerizing on or within the film.[66] The increased O═C−O feature (from C 1s) that is attributed to the increase in carbonyl, carboxylic acid, carboxylate, or carbonate species inside the film occurs with the loss of C−O and emergence of new peaks corresponding to COO^- in the FTIR spectra (Figures 3b and S2 and S3).[69] Two new peaks at 532.5 and 533.7 eV originate after 350 °C annealing (Figure 4f, from O 1s). The peak at 532.5 eV could be attributed to either hafnium silicate or C−O. However, Si was not observed in the XP spectra so we attribute this feature to C−O.[60] The peak at 533.7 eV is attributed to the presence of oxygen in carbonate species.[70−72] The main peaks present in the as-deposited samples also showed a slight shift (0.3 eV) to lower binding energies. The origins of binding energy shift could be due to several factors such as charge-transfer effects, presence of electric fields, environmental charge density, and hybridization.[73,74] Overall, the XPS data of the hafnicone films annealed at 350 °C and the annealed hafnia films are similar, indicating that the film chemistries are similar between the hafnia and thermally processed hafnicone.

The dry etch rate is important for material processing during IC manufacturing and also provides insights into film chemistry and density. The CF_4/O_2 etch rate of the as-deposited and annealed hafnicone films was compared with those of hafnia films in the as-deposited and annealed cases (Figure 5). The etch rate of the hafnicone films decreased

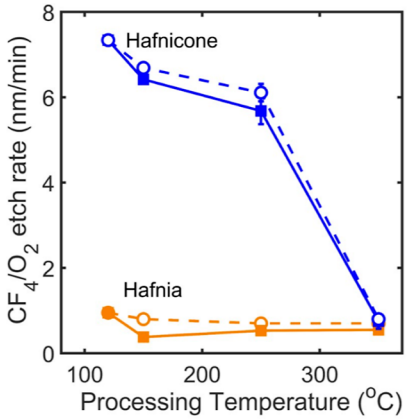

Figure 5. Dry etch rate in CF_4/O_2 plasma of the as-deposited and thermally processed hafnia and hafnicone films as a function of the annealing temperature. Both hafnia and hafnicone films were deposited at 120 °C. The hollow markers and dotted line indicate the only annealed samples, whereas the solid markers and solid line represent the UV annealed samples.

monotonically from 7.6 to 1 nm/min. The etch rate of the hafnicone films was higher than that of the hafnia films up until the 350 °C anneal temperature, at which point the etch rates were nearly identical. The etch rate of the hafnia films was nearly constant in the 0.5−1 nm/min range. The massive decrease in the etch rate in hafnicone films is correlated with film densification and the removal of organics, as described above. Removal of organics leads to mass loss, thickness decreases, and density gains, which result in chemically more stable films.

The change in the relative permittivity (k) of a material with thermal processing gives valuable insights on the evolution of film density and chemistry with thermal processing and is a key criterion for suitability in low and high-k IC applications. The dielectric constant of the as-deposited, annealed hafnia and hafnicone films was measured by fabricating MOSCAPs on Si (Figure 6). The dielectric constant of the hafnia films was higher than that of the annealed hafnicone films at all temperatures. The dielectric constant of hafnia decreased with increasing annealing temperature, whereas the dielectric constant of hafnicone increased with increasing annealing temperature. The decreases in hafnia dielectric constant can be attributed to the formation of monoclinic crystalline domains with increasing temperature, which has lower dielectric constant compared to amorphous hafnia.[75] The slight increase in the dielectric constant of the hafnicone films can be attributed to film densification and possibly the creation of new OH species in the film with increasing annealing temperature, as observed by the in situ XRR and FTIR, respectively. No significant differences were observed between the UV cured and just annealed hafnia and hafnicone films dielectric constant values.

Thermal conductivity is a crucial parameter that is typically correlated with material density and the practical ability to withdraw heat from ICs. Although not measured in this work, the thermal conductivity of ALD hafnia has been previously reported to vary from 0.27 to 1.72 W/m/K, depending on the density and crystallinity of the films.[48,76−78] The thermal

https://doi.org/10.1021/acsaelm.4c00683
ACS Appl. Electron. Mater. 2024, 6, 5173−5182

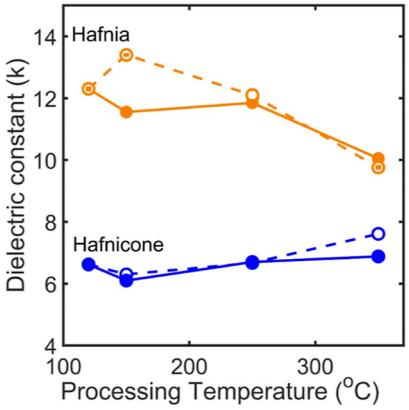

Figure 6. Evolution of the dielectric constant of the as-deposited hafnia and hafnicone films with increasing annealing temperature. Both hafnia and hafnicone films were deposited at 120 °C. The hollow markers and dotted line indicate the only annealed samples, whereas the solid markers and solid line represent the UV annealed samples.

conductivity values of the hafnicone films studied here decreased with increasing annealing temperatures up to 250 °C, followed by a significant increase after the 350 °C anneal, yet they remained on the lower end of reported values for HfO_2 (Figure 7). The initial decrease in the thermal

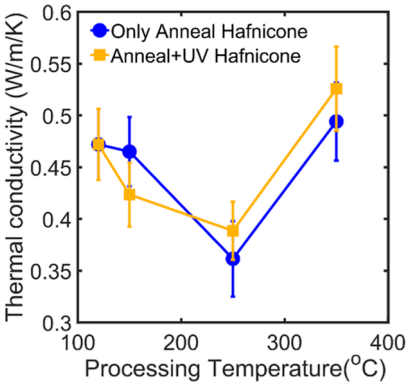

Figure 7. Thermal conductivity of the as-deposited hafnicone films with increasing annealing temperature both with and without UV exposure during anneal.

conductivity could be attributed to the removal of organics and formation of free volume which could decrease the thermal conductivity while maintaining relatively constant density and thickness.[79] An increase in the density of the hafnicone films was observed above 250 °C, accompanied by a factor of 2 decrease in the thickness over the range of annealing from 250 to 350 °C. These competing changes alone (mass loss and thickness decrease associated with densification) may not fully justify the rapid increase in thermal conductivity after the 350 °C anneal. Investigation of the FTIR spectra of hafnicone shows a near complete removal of CH_2, C−O, and COO^- vibrational peaks. This further supports the notion of a removal of organics in the film remaining from the deposition process. The densification, organic removal, and nearing the crystallization temperature of hafnicone, which would encourage a change from amorphous to crystalline structure, are all mechanisms that are consistent with the increase in thermal conductivity-associated heating from 250 to 350 °C.[76,80,81]

CONCLUSIONS

The removal of the organics from the hafnicone films with thermal treatment was observed by FTIR and XPS. Coincidently, clear increases in density and decreases in thickness were observed via in situ XRR. The removal of organics with the increase in the Hf−O−Hf bonding is observed by XPS compositional analysis. With increasing annealing temperature from 150 to 350 °C, the OH−CH_2−CH_2−O−Hf (Hf-EG) structures are decomposed, which is observed by the decrease in the intensity of −CH_x, C−C, and C−O peaks by the FTIR spectra and the decrease of Hf−O−C in the XPS C 1s spectra of hafnicone films. This decrease in intensity is accompanied by appearance of new features in the 1300−1700 cm^{-1} region after 250 °C anneal and can be attributed to the presence of symmetric and antisymmetric stretching of the carboxylate species (R−COO^-). This increase of the carboxylate species is also detected in the XPS data as the increase in the intensity of the O−C═O feature. After 350 °C anneal, the CH_x and C−C/C−O peak completely disappear, and the carboxyl peak feature appears to be stronger and was also observed in the XPS as further increase in the intensity of the O−C═O peak. Furthermore, the emergence of new peaks at 3650 cm^{-1} corresponds to the formation of new hydroxyl species that are bonded to hafnium and are isolated and not connected to other Hf−OH species via hydrogen bonding. This observation suggests that the CH_x and C−O bond cleavage leads to formation of the carboxylate species first and then to the formation of isolated Hf−OH species, as observed by FTIR and XPS Hf 4f spectra.

The as-deposited and thermally processed hafnicone films exhibited lower dielectric constant at all temperatures and higher or similar dry etch rates to those of ALD hafnia films. The exposure to UV light while annealing the hafnicone films has little to no effect on the physical, dielectric, and etch properties of hafnicone films. The hafnicone film thickness decreased, whereas density increased with annealing, but the final density of the annealed hafnicone films was lower than annealed hafnia films. The decrease in thickness and density increase is due to the removal of water and organics from the film and is evident from FTIR, thermal conductivity, and XPS compositional analysis. The presence of organics also delays the crystallization of hafnicone films as compared to ALD hafnia films as evident by in situ XRD. By thermally processing the hafnicone films, the etch rate becomes similar to the ALD hafnia films while the dielectric constant remains lower and the crystallization temperature is increased, proving that the MLD hafnicone films may be useful in low-*k* etch stops layers. MLD hybrid films were recently examined as potential candidates for negative EUV resists.[35,82] Through our work, we show that the MLD films are highly tunable via processing conditions according to the application requirements.[32] Hence, this study further supports the evidence that the thermal processing of hybrid MLD films provides an approach to design porous and/or low density materials. This approach can be used to fabricate films for applications in dielectrics, filtration, catalysis, and storage.

https://doi.org/10.1021/acsaelm.4c00683
ACS Appl. Electron. Mater. 2024, 6, 5173−5182

■ ASSOCIATED CONTENT

Supporting Information

The Supporting Information is available free of charge at https://pubs.acs.org/doi/10.1021/acsaelm.4c00683.

In situ QCM study of hafnicone growth; ex situ FTIR spectra of the as-deposited and annealed hafnicone; differential FTIR spectra of the as-deposited and annealed hafnicone films; XPS data of hafnia films; XPS composition; thickness change of ex situ annealed hafnicone films; raw in situ data of hafnia and hafnicone films with fits; ex situ XRR data of the as-deposited and annealed hafnia and hafnicone films; in situ XRR thickness and density data of hafnia and hafnicone films; porosity; thickness and refractive index of hafnicone films estimated by EMA; and *k*/density/etch rate and thermal conductivity of hafnia and hafnicone films (PDF)

■ AUTHOR INFORMATION

Corresponding Author

Nicholas C. Strandwitz − *Department of Materials Science and Engineering, Lehigh University, Bethlehem, Pennsylvania 18015, United States;* orcid.org/0000-0001-6159-9430; Email: strand@lehigh.edu

Authors

Vamseedhara Vemuri − *Department of Materials Science and Engineering, Lehigh University, Bethlehem, Pennsylvania 18015, United States;* orcid.org/0000-0001-5284-1803

Sean W. King − *Logic Technology Development, Intel Corporation, Hillsboro, Oregon 97124, United States;* orcid.org/0000-0001-5400-7679

Ryan Thorpe − *Institute for Functional Materials and Devices, Lehigh University, Bethlehem, Pennsylvania 18015-3027, United States*

Andrew H. Jones − *Laser Thermal Analysis, Inc., Charlottesville, Virginia 22902, United States*

John T. Gaskins − *Laser Thermal Analysis, Inc., Charlottesville, Virginia 22902, United States*

Patrick E. Hopkins − *Department of Materials Science and Engineering, University of Virginia, Charlottesville, Virginia 22904, United States; Department of Physics, University of Virginia, Charlottesville, Virginia 22904, United States*

Complete contact information is available at: https://pubs.acs.org/10.1021/acsaelm.4c00683

Notes

The authors declare no competing financial interest.

■ ACKNOWLEDGMENTS

The authors would like to thank Intel corporation for funding. The authors thank Nolan Sornson for assisting with building the UV cure chamber. P.E.H. appreciates support from the National Science Foundation, grant number 2318576.

■ REFERENCES

(1) Ratnesh, R. K.; Goel, A.; Kaushik, G.; Garg, H.; Chandan; Singh, M.; Prasad, B. Advancement and Challenges in MOSFET Scaling. *Mater. Sci. Semicond. Process.* **2021**, *134*, 106002.

(2) Ieong, M.; Doris, B.; Kedzierski, J.; Rim, K.; Yang, M. Silicon Device Scaling to the Sub-10-Nm Regime. *Science* **2004**, *306* (5704), 2057−2060.

(3) Banerjee, K.; Amerasekera, A.; Dixit, G.; Hu, C. The Effect of Interconnect Scaling and Low-k Dielectric on the Thermal Characteristics of the IC Metal. *International Electron Devices Meeting. Technical Digest*, 1996, pp 65−68.

(4) Shamiryan, D.; Abell, T.; Iacopi, F.; Maex, K. Low-k Dielectric Materials. *Mater. Today* **2004**, *7* (1), 34−39.

(5) Volksen, W.; Miller, R. D.; Dubois, G. Low Dielectric Constant Materials. *Chem. Rev.* **2010**, *110* (1), 56−110.

(6) Luo, Y.; Subbarayan, G. A Study of Multiple Singularities in Multi-Material Wedges and Their Use in Analysis of Microelectronic Interconnect Structures. *Eng. Fract. Mech.* **2007**, *74* (3), 416−430.

(7) Lanckmans, F.; Gray, W. D.; Brijs, B.; Maex, K. A Comparative Study of Copper Drift Diffusion in Plasma Deposited A-SiC:H and Silicon Nitride. *Microelectron. Eng.* **2001**, *55* (1−4), 329−335.

(8) Shieh, J.-M.; Tsai, K.-C.; Dai, B.-T. Low Hydrogen Content in Trimethylsilane-Based Dielectric Barriers Deposited by Inductively Coupled Plasma. *Appl. Phys. Lett.* **2002**, *81* (7), 1294−1296.

(9) Shieh, J.-M.; Tsai, K.-C.; Dai, B.-T. Ultralow Copper Drift in Inductively Coupled Plasma Silicon Carbide Dielectrics. *Appl. Phys. Lett.* **2003**, *82* (12), 1914−1916.

(10) King, S. W.; Bielefeld, J.; Xu, G.; Lanford, W. A.; Matsuda, Y.; Dauskardt, R. H.; Kim, N.; Hondongwa, D.; Olasov, L.; Daly, B.; et al. Influence of Network Bond Percolation on the Thermal, Mechanical, Electrical and Optical Properties of High and Low-k a-SiC:H Thin Films. *J. Non-Cryst. Solids* **2013**, *379*, 67−79.

(11) King, S. W. Plasma Enhanced Atomic Layer Deposition of SiNx:H and SiO2. *J. Vac. Sci. Technol., A* **2011**, *29* (4), 041501.

(12) Parsons, G. N.; Souk, J. H.; Batey, J. Low Hydrogen Content Stoichiometric Silicon Nitride Films Deposited by Plasma-enhanced Chemical Vapor Deposition. *J. Appl. Phys.* **1991**, *70* (3), 1553−1560.

(13) Dupont, G.; Caquineau, H.; Despax, B.; Berjoan, R.; Dollet, A. Structural Properties of N-Rich a-Si - N:H Films with a Low Electron-Trapping Rate. *J. Phys. D Appl. Phys.* **1997**, *30* (7), 1064−1076.

(14) Chiang, C.-C.; Chen, M.-C.; Ko, C.-C.; Jang, S.-M.; Yu, C.-H.; Liang, M.-S. Physical and Barrier Properties of Plasma-Enhanced Chemical Vapor Deposited α-SiCN:H Films with Different Hydrogen Contents. *Jpn. J. Appl. Phys.* **2003**, *42* (Part 1, No. 8), 5246−5250.

(15) Fainer, N.; Rumyantsev, Y.; Kosinova, M.; Maximovski, E.; Kesler, V.; Kirienko, V.; Kuznetsov, F. Low-k Dielectrics on Base of Silicon Carbon Nitride Films. *Surf. Coat. Technol.* **2007**, *201* (22−23), 9269−9274.

(16) Mallikarjunan, A.; Johnson, A. D.; Matz, L.; Vrtis, R. N.; Derecskei-Kovacs, A.; Jiang, X.; Xiao, M. Silicon Precursor Development for Advanced Dielectric Barriers for VLSI Technology. *Microelectron. Eng.* **2012**, *92*, 83−85.

(17) Tu, H.-E.; Chen, Y.-H.; Leu, J. Low-k SiCxNy Films Prepared by Plasma-Enhanced Chemical Vapor Deposition Using 1,3,5-Trimethyl-1,3,5-Trivinylcyclotrisilazane Precursor. *J. Electrochem. Soc.* **2012**, *159* (5), G56−G61.

(18) King, S. W. Dielectric Barrier, Etch Stop, and Metal Capping Materials for State of the Art and beyond Metal Interconnects. *ECS J. Solid State Sci. Technol.* **2015**, *4* (1), N3029−N3047.

(19) Ding, Z. J.; Wang, Y. P.; Liu, W. J.; Ding, S. J.; Baklanov, M. R.; Zhang, D. W. Characterization of PECVD Ultralow Dielectric Constant Porous SiOCH Films Using Triethoxymethylsilane Precursor and Cinene Porogen. *J. Phys. D Appl. Phys.* **2018**, *51* (11), 115103.

(20) Chang, W.-Y.; Chung, H.-T.; Chen, Y.-C.; Leu, J. Broadband UV-Assisted Thermal Annealing of Low-k Silicon Carbonitride Films Using a C-Rich Silazane Precursor. *J. Vac. Sci. Technol., B: Nanotechnol. Microelectron.: Mater., Process., Meas., Phenom.* **2018**, *36* (6), 060601.

(21) Shioya, Y.; Ohdaira, T.; Suzuki, R.; Seino, Y.; Omote, K. Effect of UV Anneal on Plasma CVD Low-k Film. *J. Non-Cryst. Solids* **2008**, *354* (26), 2973−2982.

(22) Hosseini, M.; Koike, J. Amorphous CoTix as a Liner/Diffusion Barrier Material for Advanced Copper Metallization. *J. Alloys Compd.* **2017**, *721*, 134−142.

(23) Mannaert, G.; Baklanov, M. R.; Le, Q. T.; Travaly, Y.; Boullart, W.; Vanhaelemeersch, S.; Jonas, A. M. Minimizing Plasma Damage and in Situ Sealing of Ultralow-k Dielectric Films by Using Oxygen Free Fluorocarbon Plasmas. *J. Vac. Sci. Technol., B: Microelectron. Nanometer Struct.–Process., Meas., Phenom.* **2005**, *23* (5), 2198−2202.
(24) Takahashi, H.; Takimoto, Y.; Masuda, M.; Ando, Y. Evaluation of Plasma Damage in Ultra-Low-k Materials with Cap Film Using "Extracted k-Value" Method. *Microelectron. Eng.* **2008**, *85* (10), 2107−2110.
(25) Bao, J.; Shi, H.; Liu, J.; Huang, H.; Ho, P. S.; Goodner, M. D.; Moinpour, M.; Kloster, G. M. Mechanistic Study of Plasma Damage of Low k Dielectric Surfaces. *J. Vac. Sci. Technol., B: Microelectron. Nanometer Struct.–Process., Meas., Phenom.* **2008**, *26*, 219−226.
(26) Puurunen, R. L.; Kattelus, H.; Suntola, T. Atomic Layer Deposition in MEMS Technology. *Handb. Silicon Based MEMS Mater. Technol.* **2010**, 433−446.
(27) Puurunen, R. L.; Delabie, A.; Van Elshocht, S.; Caymax, M.; Green, M. L.; Brijs, B.; Richard, O.; Bender, H.; Conard, T.; Hoflijk, I.; et al. Hafnium Oxide Films by Atomic Layer Deposition for High-κ Gate Dielectric Applications: Analysis of the Density of Nanometer-Thin Films. *Appl. Phys. Lett.* **2005**, *86* (7), 073116.
(28) Gusev, E. P.; Cabral, C.; Copel, M.; D'Emic, C.; Gribelyuk, M. Ultrathin HfO2 Films Grown on Silicon by Atomic Layer Deposition for Advanced Gate Dielectrics Applications. *Microelectron. Eng.* **2003**, *69* (2−4), 145−151.
(29) Zhang, L.; Liu, M.; Ren, W.; Zhou, Z.; Dong, G.; Zhang, Y.; Peng, B.; Hao, X.; Wang, C.; Jiang, Z. D.; et al. ALD Preparation of High-k HfO2 Thin Films with Enhanced Energy Density and Efficient Electrostatic Energy Storage. *RSC Adv.* **2017**, *7* (14), 8388−8393.
(30) Liu, X.; Ramanathan, S.; Longdergan, A.; Srivastava, A.; Lee, E.; Seidel, T. E.; Barton, J. T.; Pang, D.; Gordon, R. G. ALD of Hafnium Oxide Thin Films from tetrakis(ethylmethylamino)hafnium and Ozone. *J. Electrochem. Soc.* **2005**, *152*, G213−G219.
(31) Lee, B. H.; Yoon, B.; Anderson, V. R.; George, S. M. Alucone Alloys with Tunable Properties Using Alucone Molecular Layer Deposition and Al 2O 3 Atomic Layer Deposition. *J. Phys. Chem. C* **2012**, *116* (5), 3250−3257.
(32) Vemuri, V.; King, S. W.; Lanford, W. A.; Gaskins, J. T.; Hopkins, P. E.; Van Derslice, J.; Li, H.; Strandwitz, N. C. Comprehensive Study of the Chemical, Physical, and Structural Evolution of Molecular Layer Deposited Alucone Films during Thermal Processing. *Chem. Mater.* **2023**, *35* (5), 1916−1925.
(33) Bergsman, D. S.; Baker, J. G.; Closser, R. G.; MacIsaac, C.; Lillethorup, M.; Strickler, A. L.; Azarnouche, L.; Godet, L.; Bent, S. F. Structurally Stable Manganese Alkoxide Films Grown by Hybrid Molecular Layer Deposition for Electrochemical Applications. *Adv. Funct. Mater.* **2019**, *29* (43), 1904129.
(34) Richey, N. E.; Borhan, S.; Bent, S. F. Multi-Metal Coordination Polymers Grown through Hybrid Molecular Layer Deposition. *Dalton Trans.* **2021**, *50* (13), 4577−4582.
(35) Shi, J.; Ravi, A.; Richey, N. E.; Gong, H.; Bent, S. F. Molecular Layer Deposition of a Hafnium-Based Hybrid Thin Film as an Electron Beam Resist. *ACS Appl. Mater. Interfaces* **2022**, *14* (23), 27140−27148.
(36) Ghazaryan, L.; Kley, E.-B.; Tünnermann, A.; Viorica Szeghalmi, A. Stability and Annealing of Alucones and Alucone Alloys. *J. Vac. Sci. Technol., A* **2012**, *31* (1), 01A149.
(37) DuMont, J. W.; George, S. M. Pyrolysis of Alucone Molecular Layer Deposition Films Studied Using In Situ Transmission Fourier Transform Infrared Spectroscopy. *J. Phys. Chem. C* **2015**, *119* (26), 14603−14612.
(38) Kim, H.; Hyun, J.; Kim, G.; Lee, E.; Min, Y.-S. Origin of Instability of Titanicone Grown by Molecular Layer Deposition Using TiCl4 and Ethylene Glycol. *Chem. Mater.* **2024**, *36*, 247−255.
(39) Cho, Y.; Huang, J.; Zhang, Z.; Wang, K.; Lee, P.-C.; Kim, C.; Wong, K.; Nemani, S.; Yieh, E.; Kummel, A. C. Inherent Selective Pulsed Chemical Vapor Deposition of Aluminum Oxide in Nm Scale. *Appl. Surf. Sci.* **2023**, *622*, 156824.
(40) Lee, S.; Lee, J.; Yang, J.; Choi, T. Study of Etch Stop Layer on Characteristics of Amorphous Aluminum Oxide Thin Film. *ECS Meet. Abstr.* **2022**, *MA2022-01* (21), 2433.
(41) Lee, B. H.; Anderson, V. R.; George, S. M. Growth and Properties of Hafnicone and HfO2/Hafnicone Nanolaminate and Alloy Films Using Molecular Layer Deposition Techniques. *ACS Appl. Mater. Interfaces* **2014**, *6* (19), 16880−16887.
(42) Ju, L.; Vemuri, V.; Strandwitz, N. C. Quartz Crystal Microbalance Study of Precursor Diffusion during Molecular Layer Deposition Using Cyclic Azasilane, Maleic Anhydride, and Water. *J. Vac. Sci. Technol., A* **2019**, *37* (3), 030909.
(43) Kern, W. Evolution of Silicon Wafer Cleaning Technology. *J. Electrochem. Soc.* **1990**, *137* (6), 1887.
(44) Baer, D. R.; Artyushkova, K.; Cohen, H.; Easton, C. D.; Engelhard, M.; Gengenbach, T. R.; Greczynski, G.; Mack, P.; Morgan, D. J.; Roberts, A. XPS Guide: Charge Neutralization and Binding Energy Referencing for Insulating Samples. *J. Vac. Sci. Technol., A* **2020**, *38* (3), 31204.
(45) Braun, J. L.; Olson, D. H.; Gaskins, J. T.; Hopkins, P. E. Steady-state thermo-reflectance method & system to measure thermal conductivity. WO 2020047054 A1, 2020. https://patents.google.com/patent/WO2020047054A1 (accessed Sept 23, 2023).
(46) Foley, B. M.; Gaskins, J. T.; Hopkins, P. E. Fiber-Optic Based Material Property Measurement System and Related Methods. U.S. Patent 11,635,376 B2, 2023.
(47) Braun, J. L.; Olson, D. H.; Gaskins, J. T.; Hopkins, P. E. A Steady-State Thermoreflectance Method to Measure Thermal Conductivity. *Rev. Sci. Instrum.* **2019**, *90* (2), 24905.
(48) Scott, E. A.; Gaskins, J. T.; King, S. W.; Hopkins, P. E. Thermal Conductivity and Thermal Boundary Resistance of Atomic Layer Deposited High- k Dielectric Aluminum Oxide, Hafnium Oxide, and Titanium Oxide Thin Films on Silicon. *APL Mater.* **2018**, *6* (5), 43.
(49) Lee, B. H.; Yoon, B.; Abdulagatov, A. I.; Hall, R. A.; George, S. M. Growth and Properties of Hybrid Organic-Inorganic Metalcone Films Using Molecular Layer Deposition Techniques. *Adv. Funct. Mater.* **2013**, *23* (5), 532−546.
(50) Dameron, A. A.; Seghete, D.; Burton, B. B.; Davidson, S. D.; Cavanagh, A. S.; Bertrand, J. A.; George, S. M. Molecular Layer Deposition of Alucone Polymer Films Using Trimethylaluminum and Ethylene Glycol. *Chem. Mater.* **2008**, *20* (10), 3315−3326.
(51) Fu, P.; Hu, S.; Xiang, J.; Li, P.; Huang, D.; Jiang, L.; Zhang, A.; Zhang, J. FTIR Study of Pyrolysis Products Evolving from Typical Agricultural Residues. *J. Anal. Appl. Pyrolysis* **2010**, *88* (2), 117−123.
(52) Fu, P.; Hu, S.; Xiang, J.; Sun, L.; Yang, T.; Zhang, A.; Zhang, J. Mechanism Study of Rice Straw Pyrolysis by Fourier Transform Infrared Technique. *Chin. J. Chem. Eng.* **2009**, *17* (3), 522−529.
(53) Hausmann, D. M.; Gordon, R. G. Surface Morphology and Crystallinity Control in the Atomic Layer Deposition (ALD) of Hafnium and Zirconium Oxide Thin Films. *J. Cryst. Growth* **2003**, *249* (1−2), 251−261.
(54) Jaffe, J. E.; Bachorz, R. A.; Gutowski, M. Low-Temperature Polymorphs of ZrO2 and HfO2: A Density-Functional Theory Study. *Phys. Rev. B: Condens. Matter Mater. Phys.* **2005**, *72*, 144107.
(55) Kidchob, T.; Malfatti, L.; Serra, F.; Falcaro, P.; Enzo, S.; Innocenzi, P. Hafnia Sol-Gel Films Synthesized from HfCl4: Changes of Structure and Properties with the Firing Temperature. *J. Sol-Gel Sci. Technol.* **2007**, *42* (1), 89−93.
(56) Lin, F.; Hoex, B.; Koh, Y. H.; Lin, J. J.; Aberle, A. G. Low-Temperature Surface Passivation of Moderately Doped Crystalline Silicon by Atomic-Layer-Deposited Hafnium Oxide Films. *Energy Procedia* **2012**, *15*, 84−90.
(57) Hendrix, E.; Garland, B. M.; Vemuri, V.; Strandwitz, N. C. Atomic Layer Deposition of MoOx Thin Films Using Mo(IPrCp)2H2 and O3. *J. Vac. Sci. Technol., A* **2023**, *41* (3), 32409.
(58) Baruch, M. F.; Pander, J. E.; White, J. L.; Bocarsly, A. B. Mechanistic Insights into the Reduction of CO2 on Tin Electrodes Using in Situ ATR-IR Spectroscopy. *ACS Catal.* **2015**, *5* (5), 3148−3156.

https://doi.org/10.1021/acsaelm.4c00683
ACS Appl. Electron. Mater. 2024, 6, 5173−5182

(59) Detweiler, Z. M.; White, J. L.; Bernasek, S. L.; Bocarsly, A. B. Anodized Indium Metal Electrodes for Enhanced Carbon Dioxide Reduction in Aqueous Electrolyte. *Langmuir* **2014**, *30* (25), 7593−7600.
(60) Kaiser, N.; Vogel, T.; Zintler, A.; Petzold, S.; Arzumanov, A.; Piros, E.; Eilhardt, R.; Molina-Luna, L.; Alff, L. Defect-Stabilized Substoichiometric Polymorphs of Hafnium Oxide with Semiconducting Properties. *ACS Appl. Mater. Interfaces* **2022**, *14* (1), 1290−1303.
(61) Kaichev, V. V.; Dubinin, Y. V.; Smirnova, T. P.; Lebedev, M. S. A Study of the Structure of (HfO2)x(Al 2O3)1-x/Si Films by X-Ray Photoelectron Spectroscopy. *J. Struct. Chem.* **2011**, *52* (3), 480−487.
(62) Barreca, D.; Milanov, A.; Fischer, R. A.; Devi, A.; Tondello, E. Hafnium Oxide Thin Film Grown by ALD: An XPS Study. *Surf. Sci. Spectra* **2007**, *14* (1), 34−40.
(63) Zhang, X. Y.; Hsu, C. H.; Cho, Y. S.; Zhang, S.; Lien, S. Y.; Zhu, W. Z.; Xiong, F. B. Rapid Thermal Processing of Hafnium Dioxide Thin Films by Remote Plasma Atomic Layer Deposition as High-k Dielectrics. *Thin Solid Films* **2018**, *660*, 797−801.
(64) Idriss, H. On the Wrong Assignment of the XPS O1s Signal at 531−532 EV Attributed to Oxygen Vacancies in Photo- and Electro-Catalysts for Water Splitting and Other Materials Applications. *Surf. Sci.* **2021**, *712*, 121894.
(65) Baek, G.; Lee, S.; Lee, J.-H.; Park, J.-S. Air-Stable Alucone Thin Films Deposited by Molecular Layer Deposition Using a 4-Mercaptophenol Organic Reactant. *J. Vac. Sci. Technol., A* **2020**, *38* (2), 22411.
(66) Hackley, J. C.; Gougousi, T. Properties of Atomic Layer Deposited HfO2 Thin Films. *Thin Solid Films* **2009**, *517* (24), 6576−6583.
(67) Zhang, W.; Kong, J. Z.; Cao, Z. Y.; Li, A. D.; Wang, L. G.; Zhu, L.; Li, X.; Cao, Y. Q.; Wu, D. Bipolar Resistive Switching Characteristics of HfO2/TiO2/HfO2 Trilayer-Structure RRAM Devices on Pt and TiN-Coated Substrates Fabricated by Atomic Layer Deposition. *Nanoscale Res. Lett.* **2017**, *12*, 393.
(68) Tan, T.; Guo, T.; Wu, Z.; Liu, Z.; Hsieh, C.-Y.; Bo, T.-C.; Tan, T.; Guo, T.; Wu, Z.; Liu, Z. Charge Transport and Bipolar Switching Mechanism in a Cu/HfO2/Pt Resistive Switching Cell*. *Chin. Phys. B* **2016**, *25* (11), 117306.
(69) Watts, J. F. High resolution XPS of organic polymers: The Scienta ESCA 300 database. G. Beamson and D. Briggs. 280pp., £65. John Wiley & Sons, Chichester, ISBN 0471 935921, (1992). *Surf. Interface Anal.* **1993**, *20* (3), 267.
(70) Lee, J. C.; Oh, S. J.; Cho, M.; Hwang, C. S.; Jung, R. Chemical Structure of the Interface in Ultrathin HfO2/Si Films. *Appl. Phys. Lett.* **2004**, *84* (8), 1305−1307.
(71) Liu, X.; Sheng, D.; Gao, X.; Yang, Y. Effect of Air Corona Discharge Irradiation on the Surface Composition and Morphology of the Polyester Film. *Acta Agron. Sin.* **2013**, *30* (07), 750.
(72) Quinlan, R. A.; Lu, Y.-C.; Kwabi, D.; Shao-Horn, Y.; Mansour, A. N. XPS Investigation of the Electrolyte Induced Stabilization of LiCoO 2 and "AlPO 4 "-Coated LiCoO 2 Composite Electrodes. *J. Electrochem. Soc.* **2016**, *163* (2), A300−A308.
(73) Bagus, P. S.; Illas, F.; Pacchioni, G.; Parmigiani, F. Mechanisms Responsible for Chemical Shifts of Core-Level Binding Energies and Their Relationship to Chemical Bonding. *J. Electron Spectrosc. Relat. Phenom.* **1999**, *100* (1−3), 215−236.
(74) Kim, M. S.; Ko, Y. D.; Yun, M.; Hong, J. H.; Jeong, M. C.; Myoung, J. M.; Yun, I. Characterization and Process Effects of HfO2 Thin Films Grown by Metal-Organic Molecular Beam Epitaxy. *Mater. Sci. Eng., B* **2005**, *123* (1), 20−30.
(75) Kumar, A.; Lee, J. Y.; Lee, S. Y. Phase Transformation of Sputtered Hafnium Oxide by Post Annealing Treatment and Its Effect on the Amorphous Si-In-Zn-O Thin Film Transistor. *J. Alloys Compd.* **2022**, *906*, 164289.
(76) Gabriel, N. T.; Talghader, J. J. Thermal Conductivity and Refractive Index of Hafnia-Alumina Nanolaminates. *J. Appl. Phys.* **2011**, *110* (4), 43526.
(77) Panzer, M. A.; Shandalov, M.; Rowlette, J. A.; Oshima, Y.; Chen, Y. W.; McIntyre, P. C.; Goodson, K. E. Thermal Properties of Ultrathin Hafnium Oxide Gate Dielectric Films. *IEEE Electron Device Lett.* **2009**, *30* (12), 1269−1271.
(78) Hinz, M.; Marti, O.; Gotsmann, B.; Lantz, M. A.; Dürig, U. High Resolution Vacuum Scanning Thermal Microscopy of Hf O2 and Si O2. *Appl. Phys. Lett.* **2008**, *92* (4), 48.
(79) Saini, S.; Mele, P.; Oyake, T.; Shiomi, J.; Niemelä, J. P.; Karppinen, M.; Miyazaki, K.; Li, C.; Kawaharamura, T.; Ichinose, A.; et al. Porosity-Tuned Thermal Conductivity in Thermoelectric Al-Doped ZnO Thin Films Grown by Mist-Chemical Vapor Deposition. *Thin Solid Films* **2019**, *685*, 180−185.
(80) Gorham, C. S.; Gaskins, J. T.; Parsons, G. N.; Losego, M. D.; Hopkins, P. E. Density Dependence of the Room Temperature Thermal Conductivity of Atomic Layer Deposition-Grown Amorphous Alumina (Al2O3). *Appl. Phys. Lett.* **2014**, *104* (25), 253107.
(81) Kim, Y.; Kwon, H.; Han, H. S.; Kim, H. J. K.; Kim, B. S. Y.; Lee, B. C.; Lee, J.; Asheghi, M.; Prinz, F. B.; Goodson, K. E.; et al. Tunable Dielectric and Thermal Properties of Oxide Dielectrics via Substrate Biasing in Plasma-Enhanced Atomic Layer Deposition. *ACS Appl. Mater. Interfaces* **2020**, *12* (40), 44912−44918.
(82) Ravi, A.; Shi, J.; Lewis, J.; Bent, S. F. Molecular Layer Deposition of an Al-Based Hybrid Resist for Electron-Beam and EUV Lithography. *Proc. SPIE 12498, Advances in Patterning Materials and Processes XL, 124981B*, 2023, pp 251−258.

https://doi.org/10.1021/acsaelm.4c00683
ACS Appl. Electron. Mater. 2024, 6, 5173−5182